General Disclaimer

One or more of the Following Statements may affect this Document

AIAA

DAA/Langley

NASA GRANT NAG-1-263

(NASA-CR-175921) MEASUREMENT OF ULTRASONIC
FIELDS IN TRANSPARENT MEDIA USING A SCANNING
DIFFERENTIAL INTERFEROMETER Final Report
(Virginia Polytechnic Inst. and State Univ.)
36 p HC A03/MF A01 CSCL 20A G3/71

N85-28726

Unclas
23761

MEASUREMENT OF ULTRASONIC FIELDS IN TRANSPARENT MEDIA USING A SCANNING DIFFERENTIAL INTERFEROMETER

G. Daniel Dockery and Richard O. Claus
Department of Electrical Engineering
Virginia Polytechnic Institute and State University
Blacksburg, VA 24061

ABSTRACT

An experimental system for the detection of three-dimensional acoustic fields in optically transparent media using a dual beam differential interferometer is described. In this system, two coherent, parallel, focused laser beams are passed through the specimen and the interference fringe pattern which results when these beams are combined shifts linearly by an amount which is related to the optical pathlength difference between the two beams. It is shown that for small signals, the detector output is directly proportional to the amplitude of the acoustic field integrated along the optical beam path through the specimen. A water tank and motorized optical platform have been constructed to allow these dual beams to be scanned through an ultrasonic field generated by a piezoelectric transducer at various distances from the transducer. Scan data for the near, Fresnel, and far zones of a uniform, circular transducer are presented and an algorithm for constructing the radial field profile from this integrated optical data, assuming cylindrical symmetry, is described. This algorithm is applied to both averaged and smoothed scan data and qualitative agreement between the measurements and analytic predictions is demonstrated.

I. INTRODUCTION

There are several different techniques available for the detection of bulk ultrasonic fields in liquids, including systems which utilize both contact and non-contact transducers as receivers [1]. Contact transducers are often piezoelectric crystals which are scanned through the field to map its amplitude. Although the use of piezoelectric transducers as receivers is simple, there are some disadvantages associated with this approach including the disruption of the field in the vicinity of the receiving transducer and the possibility of poor resolution due to the relatively large size of the receiver with respect to acoustic wavelength. On the other hand, in transparent materials, the use of a probing optical beam as a non-contact transducer has several advantages including direct measurement of the refractive index of the field and the potential for excellent spatial resolution.

Within the category of narrow beam optical probing, there are two classes of simple systems; 1) knife-edge systems and 2) interferometer systems [1]. Knife edge techniques measure deflections in the probing beam which, in the case of bulk wave measurements, result from refraction as the beam passes through regions of differing refractive index.

In interferometric systems, one or both of the interferometer beams or "arms" pass through the bulk of the specimen, and the optical pathlength difference between these beams is monitored. Again, measured pathlength differences result when the sampling arm passes through the areas of different refractive index which are produced by the ultrasonic field. Both systems give adequate results, but measurements obtained with the interferometer system are mathematically easier to relate to the pressure field in the medium.

II. DIFFERENTIAL INTERFEROMETER

A. THEORY OF OPERATION

The interferometer discussed here is a variation of the type of system developed by Palmer and coworkers and Jablonowski for the detection of surface waves [3,6]. In the present applicaton, both beams are passed through a water tank and the detector output is proportional to the relative pathlength difference of the two beams. Figure 1 contains a layout of the system showing the relative positions of the major components. Because both beams travel the same distance in the water, the difference in their optical pathlengths arises soley from a difference in the average index of refraction that the beams encounter while they are in the water. As a first approximation, the refractive index is assumed to be linearly related to the acoustic pressure in the water.

After travelling through the water tank, and thus through the ultrasonic field, the beams are recombined and an interference fringe pattern results. Assume that the two converging beams make an angle θ with each other, where θ is defined in Figure 2. Then, the beams can be represented mathematically as

$$E_1 = E_o \exp(i[\omega t - k(x\sin\theta + z\cos\theta) - kn_1 d]), \text{ and} \tag{1}$$

$$E_2 = E_o \exp(i[\omega t - k(-x\sin\theta + z\cos\theta) - kn_2 d]), \tag{2}$$

where

$k = 2\,/\lambda$ = wavenumber of light,

λ = wavelength of light,

ω = angular frequency of light,

d= distance beams travel in water, and

n_1, n_2 = average refractive indices experienced by beams 1 and 2, respectively.

In the region where the beams overlap, the electric field is given by

$$E = E_1 + E_2$$

$$= E_o e^{i(\omega t - kz\cos\theta)} \left\{ e^{ik(x\sin\theta - n_2 d)} + e^{-ik(x\sin\theta + n_1 d)} \right\} \tag{3}$$

This expression can be rewritten in terms of the difference of the two average indices, $\Delta n = n_1 - n_2$, with the result

$$E = 2E_o e^{i\left\{\omega t - kz\cos\theta - \frac{kd}{2}(n_1+n_2)\right\}} \cos\left[k\left(x\sin\theta + \tfrac{1}{2}\Delta nd\right)\right]. \tag{4}$$

Of course, the detector responds to the optical irradiance which is found to be

$$I = EE^* = 4\, E_o^2 \cos^2\left[k\left(x\sin\theta + \tfrac{1}{2}\Delta nd\right)\right], \tag{5}$$

or, for small θ,

$$I \approx 4\, E_o^2 \cos^2\left[k\left(x\theta + \frac{1}{2}\,\Delta nd\right)\right]. \tag{6}$$

Equation (6) describes a fringe pattern in the x-direction with maximum intensities occurring at locations given by

$$x_{max} = \frac{1}{2\theta}(m\lambda - \Delta nd) \qquad (7)$$

Similarly, the locations of the minimum values of intensity are given by

$$x_{min} = \frac{1}{2\theta}\left(\frac{(2m-1)}{2}\lambda - \Delta nd\right). \qquad (8)$$

The fringe spacing is obtained by subtracting the positions of successive maxima:

$$\Delta x = \frac{1}{2\theta}([(m+1)\lambda - \Delta nd] - (m\lambda - \Delta nd))$$

$$= \lambda/2\theta. \qquad (9)$$

According to (7) the result of a change in the relative phases of the beams is a linear shift in the position of the fringe pattern. According to (9), however, this shift is not accompanied by a change in the fringe spacing.

Detection of the shifting fringes is accomplished with the aid of a Ronchi ruling (square-wave grating) which is used to spatially demodulate the light. The calculation to determine the transmitted power involves integrating the irradiance over a single slit and then summing the contributions from the remaining slits [5]. Under the assumption that the signal is small, which is usually the case, the following expression can be found for the power incident on the detector:

$$P = P_o/2 - P_o(2\Delta nd/\lambda), \tag{10}$$

where P_o is the total incident power in the optical beams. In (10), $P_o/2$ is a dc-term so the varying contribution changes linearly with Δn. Therefore, under the assumptions noted in this discussion, this interferometer produces an output signal which is directly proportional to the acoustic pressure field.

B. OPTICAL HARDWARE IMPLEMENTATION

Most of the critical components in this system are dedicated to producing the dual, equal intensity, parallel laser beams which are to be directed through the water tank shown in Figure 1. Toward this end, the original laser beam is expanded in a collimator and passed through a Ronchi ruling. A spatial Fourier transform is performed on the resulting signal by convex lens L1 and the transform pattern is incident on a spatial filter which allows only the + and - first orders to pass. The output of this filter is two smaller, coherent beams whose separation is determined by the spacing of the Ronchi grating. These beams are then passed through a vari-focal system of three lenses (L2 through L4) which cause the beams to be parallel to each other and individually focused. Varying the relative positions of the three lenses controls the minimum spot size, the length of the focal region, and the separation of the two beams.

For maximum sensitivity in the detection of continuous wave acoustic fields, the beam separation should be an odd integer number of half acoustic wavelengths. In this case, assuming the beams are parallel to the ultrasonic plane wave fronts, when one beam is traversing a plane of maximum compression, the other beam is sampling a plane of maximum rarefaction. The beam separation is not as critical in pulsed wave detection because, for a minimum separation of a few acoustic wavelengths, one beam is always measuring the equilibrium pressure while the other is detecting the passage of the pulse.

After emerging from the water, the two beams are focused together onto a microscope objective by L5. The separation of the beams and the focal length of L5 determine the angle with which the beams come together and, as discussed in the previous section, this determines the fringe spacing of the interference pattern. The microscope objective causes the beams to remain superimposed on each other for the remainder of their optical pathlengths. A Ronchi ruling is placed at the proper position to spatially demodulate the fringe pattern and a relatively broad set of fringes results. An adjustable iris is used to filter all but one of these larger fringes and the output is focused on the detector photodiode by L6.

III. EXPERIMENTAL SCANNING SYSTEM

A. OPTICAL PLATFORM AND WATER TANK

Compressional waves produced by a 7.62 cm diameter x-cut quartz transducer dimensioned to resonate at 500 kHz were propagated in a large water tank constructed primarily of glass and plexiglass. Uniform electroding on both sides of the transducer was used to generate an acoustic field whose propagation in the tank could be easily modeled. Suspended above the tank on aluminum rails is a plexiglass optical platform with the detecting optical system mounted on it. Arrangement of the tank and platform is illustrated in Figure 3. Precision movements of the optical system are accomplished using a CCS series 2200 microprocessor, a Cybernetics CY500 motor controller, and a Superior Electric MD093-FD11 stepper motor. The platform has sufficient vertical travel to allow the optical beams to scan the entire cross section of the tank.

The inside of the tank measures 35 cm wide, 35 cm high, and 168 cm long. This fairly long propagation distance is necessary because radiation from the large, low frequency source must travel 75 to 100 centimeters to reach the far-field. Angled sides coming to a point are used at the front of the tank to reduce unwanted reflections of the ultrasonic waves. This arrangement works well enough to make the use of acoustic absorbing material on the walls unnecessary. The tank sides through which the optical beams pass are 0.6 cm thick BK7 optical glass.

Because the relative positions of the tank and platforms are fixed, measurements at different distances from the source are made by moving the transducer along the length of the tank. This is accomplished by suspending the plexiglass plate, which holds the transducer, from a threaded rod mounted longitudinally on the tank.

Figure 4 is a schematic layout of the optical platform; the layout shown corresponds to the dual beam differential interferometer discussed above. The platform is fabricated out of plexiglass with five centimeter aluminum angle added for stiffening. Adjustable 1.25 cm aluminum angle rails are attached to the platform for optical alignment. The system is tuned by sliding components along these rails, adjusting mirrors M1 through M4, and rotating gratings G1 and G2. Also, the pin holes, which filter the Fourier transform pattern of the grating, are fixed in a translation stage which moves in both transverse directions. The total optical path length of the system, with no water in the tank, is approximately 250 centimeters.

B. DATA ACQUISITION

A schematic block diagram of the data acquisition system is given in Figure 5. The CCS microprocessor is used to command the CY500 motor controller which, in turn, drives the main power amplifiers for the stepper motor. The motor output shaft is connected to a ten-to-one reduction gear box with a spool and optical platform cable attached to it. This arrangement allows positioning of the scanning optical beams to within 0.034 mm. Software for the microprocessor is designed to provide storage for data entered by the operator as well as to automatically advance the optical platform some predetermined amount. In this way, it is possible to make repeated scans over the same portion of the tank without positioning errors.

The output signal from the detector is passed through a 40 dB amplifier and then through a high-pass filter to eliminate residual low frequency noise which results from table vibrations. In the current arrangement, this signal is read from an oscilloscope and then entered into the microprocessor. After completing the desired scans, the data is transferred to a larger IBM system for processing using the reconstruction algorithm described in the next section.

C. FIELD RECONSTRUCTION ALGORITHM

One of the major difficulties associated with optical techniques in the detection of bulk waves is that the beams integrate all the refractive index contributions along their paths through the specimen. The resulting signal is proportional to a difference in the average index of refraction experienced by the two beams. It remains, then, to use this integrated data to reconstruct the actual two-dimensional ultrasonic field profile. In a comprehensive article on reconstruction techniques, Sweeney and Vest describe and compare six different methods for reconstructing refractive index fields from interferometric data [7]. Unfortunately, none of the approaches they discuss are applicable to the measurements discussed here because each of the algorithms requires multidirectional or holographic data where the angle of beam incidence is varied. Such data, of course, is not provided by the one-dimensional scans which are conducted in this work.

It is possible, however, to attempt a simple reconstruction using this data when cylindrical symmetry of the ultrasonic field is assumed. This is done by dividing the field into annular rings of resolution and subtracting the contributions of previously measured rings as the optical beam moves deeper into the acoustic field. An illustration of the problem is provided in Figure 6 and the analysis which leads to the development of the algorithm is presented below.

As shown in Figure 6, the cylindrically symmetric acoustic field is represented by adjacent annular rings of constant field amplitude and width w. For maximum applicability, w should be on the order of the diameter of the optical beam. If a scan produces N non-zero measurements, then the following expressions define the angles γ_{1ij} and γ_{2ij}:

$$\cos\gamma_{1ij} = \frac{N - \frac{2j-1}{2}}{N-i}\text{, and} \tag{11}$$

$$\cos\gamma_{2ij} = \frac{N - \frac{2j-1}{2}}{N-i+1}\text{,}$$

where the subscripts refer to the jth measurement and the ith annular ring. Using these relations, it is possible to solve for the pathlengths of the beams through each ring for each measurement. For example, the distance the beam travels through the central section of the jth ring (this case corresponds to i=j) is given by

$$d_{mj} = w\left(N - \frac{2j-1}{2}\right)\tan\gamma_{2ij}. \tag{13}$$

Similarly, the distance the optical beam travels through non-central sections of the rings is found to be

$$d_{ij} = w\left(N - \frac{2j-1}{2}\right)(\tan\gamma_{2ij} - \tan\gamma_{1ij}). \tag{14}$$

In effect, this method solves for the average index of refraction in the center sections in the rings and, because the size of this central region decreases toward the middle of the field, the resolution of the scheme increases toward the middle of the field. The general algorithm is developed as follows: it is assumed that the first field point is related to the first measurement according to

$$f_1 = \frac{\phi_1}{2\, d_{m1}} , \tag{15}$$

where f_1 is the field amplitude and ϕ_1 is the first measurement. Successive measurements are then expressed as combinations of previous field values such that

$$\begin{aligned}
\phi_2 &= 2d_{12}f_1 + 2d_{m2}f_2 \\
\phi_3 &= 2d_{13}f_1 + 2d_{23}f_2 + 2d_{m3}f_3 \\
\phi_4 &= 2d_{14}f_1 + 2d_{24}f_2 + 2d_{34}f_3 + 2d_{m4}f_4 \\
&\vdots \\
\phi_j &= 2\sum_{i=1}^{j-1} d_{ij}f_i + 2d_{mj}f_i \ .
\end{aligned} \tag{16}$$

Equation (16) is solved for the jth field point with the result

$$f_j = \frac{\phi_j - 2 \sum_{i=1}^{j-1} dij\ fi}{2d_{mj}} \ . \tag{17}$$

This expression is the basis of the reconstruction scheme since it can be used to sequentially calculate the amplitude at every point along the radius of the ultrasonic field.

The algorithm presented here has three basic disadvantages, the most obvious of which is the restrictive assumption of cylindircal symmetry. In addition to this, however, implementation of this scheme requires that one determine the first non-zero measurement (above noise, for example) and also the center of the field relative to the first non-zero measurement. Fortunately, the raw data can be plotted and examined to find these points before any reconstruction is attempted. Despite these shortcomings this algorithm is simple to apply and has been used successfully to reconstruct fields generated by circular tranducers in water. Specific examples are presented in the next section.

IV. RESULTS

For the measurements presented here, the piezoelectric transducer was driven by a MetroTek MP215 pulser which is pulsed at a rate of approximately 5 kHz. A typical output signal from the detector is shown in Figure 7. The first small spike, marked a, is the inductively coupled signal. The distance, or time, between this spike and the first acoustic peak, marked b, corresponds to the distance between the transducer and the optical beams. Peaks b and c result when the acoustic pulse reaches the first and second beams, respectively. As stated above, when operating in a pulsed mode, one beam is always acting as a reference arm while the other beam measures the pulse. The maximum value of these peaks is directly proportional to the optical pathlength difference between the beams and is the quantity which must be recorded at each scan position.

All of the data presented in this section are the result of scans in the far-field of an 8 cm diameter, uniform transducer. Although the transducer is pulsed, Figure 7 indicates that the crystal "rings" at its resonant frequency for several cycles after the initial pulse. The resulting pulse-packet contains a sufficient number of oscillations to cause the far-field pattern to have some of the structure predicted for continuous-wave operation.

Two types of scans were made; one which passed through the entire diameter of the field and another which made only a radial pass. Several scans of each type were made so that averaging and comparisons could be carried out. Figure 8 contains typical data for a diameter scan and Figure 9 is a smoothed average of five such scans. The smoothing, which was accomplished using simple three point averaging, was necessary because the reconstruction routine proved to be quite sensitive to the amplitude discretization which results when reading the data from an oscilloscope. After subtracting the noise level from the data of Figure 9, half of the data points were entered into the reconstruction algorithm in (17) with the result given in Figure 10. This plot shows clear evidence of the sidelobe structure predicted for the far-field pattern of a uniform circular transducer.

In Figure 11, typical raw data from a radius scan is presented. These scans contain the same number of data points as the diameter scans and were intended to resolve more of the sidelobe structure. Figure 12 contains a smoothed five-scan average of this type of data. In this case, five point averaging was used to accomplish the smoothing. All but the last few data points were read in to the reconstruction algorithm and the result is shown in Figure 13. It appears that the sidelobe resolution is somewhat improved in this example. It is worth noting that all the scans, with or without averaging, produce reconstructed field profiles which are very similar to the examples presented here. Some smoothing, however, proves to be necessary in all cases.

V. CONCLUSION

A dual beam differential interferometer, which has been designed and built to detect acoustic waves in water, is used for measurements in the far-field of a uniform, circular transducer. Several scans are taken through the diameter and radius of the ultrasonic field and the data is seen to be reproducible. Reconstruction of the integrated measurements is successfully accomplished using an algorithm which assumes cylindrical symmetry in the ultrasonic field. The processed data which is generated by the reconstruction routine represents a radial profile of the field amplitude at that particular distance from the transducer. Reconstructions of the data taken with this interferometric system indicate that the field profile contains the general shape, including sidelobes, which is expected in the far-field of a uniform circular source. Furthermore, the radius scans, which use a smaller step-size, reveal more detail in the field profile than do the diameter scans.

VI. ACKNOWLEDGEMENTS

The authors thank J. Gray and R. Burrier for their assistance. This work was partially supported by NASA Grant NAG-1-263.

REFERENCES

1. W. Sachse and N. N. Nsu, "Ultrasonic transducers for materials testing and their characterization," in *Physical* Acoustics, vol. 14, W. P. Mason and R. N. Thurston, eds., Academic Press (New York), 1979.

2. G. I. Stegman, "Optical probing of surface waves and surface wave devices," IEEE Trans. Sonics Ultrason. SU-23, 33(1976).

3. C. H. Palmer, "Ultrasonic surface wave detection by optical interferometry," J. Acoust. Soc. Am. 53, 948(1973).

4. C. H. Palmer, H. M. South, and T. H. Mak, "Optical interferometry for measurement of Rayleigh and dilitational waves," Ultrasonics 11, 106(1974).

5. C. H. Palmer, R. O. Claus and S. E. Fick, "Ultrasonic wave measurement by differential interferometry," Appl. Opt. 16, 1849(1977).

6. D. P. Jablonowski, "Simple interferometer for monitoring Rayleigh waves," Appl. Opt. 17, 2064(1978).

7. D. W. Sweeney and C. M. Vest, "Reconstruction of three-dimensional refracive index fields from multidirectional interferometric data," Appl. Opt. 12, 2649(1973).

FIGURE TITLES

Fig. 1. Dual beam differential interferometer.

Fig. 2. Geometry of optical beam recombination.

Fig. 3. Arrangement of optical platform and water tank.

Fig. 4. System design of components and optical platform.

Fig. 5. Block diagram of data acquisition system.

Fig. 6. Acoustic field reconstruction geometry.

Fig. 7. Typical optical detector output signal.

Fig. 8. Data from far-field diameter scan of ultrasonic field.

Fig. 9. Smoothed average of five diameter scan of ultrasonic field.

Fig. 10. Field reconstructed from averaged diameter scan data.

Fig. 11. Data from far-field radius scan of ultrasonic field.

Fig. 12. Smoothed average of five radius scans.

Fig. 13. Field reconstructed from averaged radius scan data.

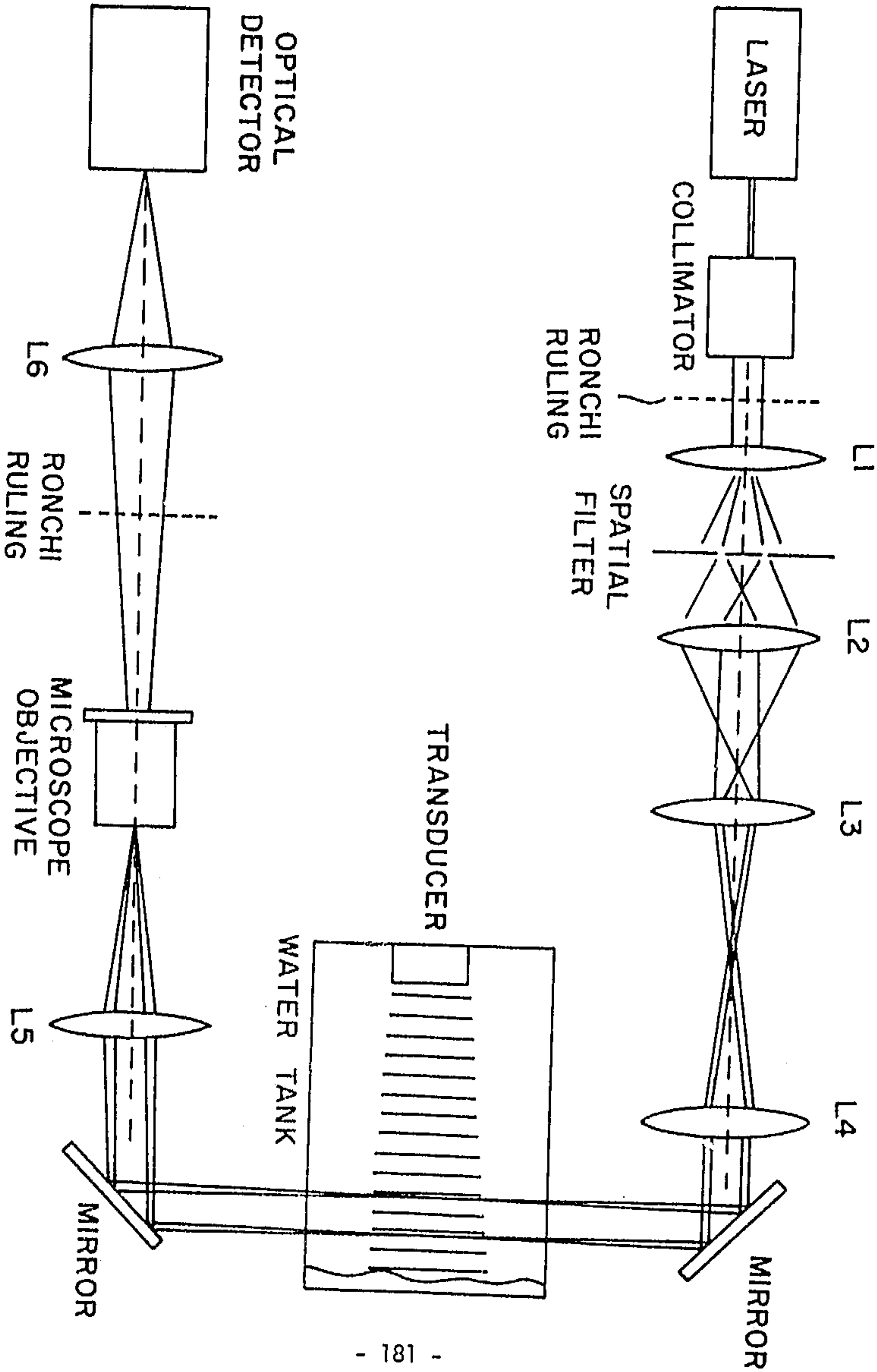
LASER
COLLIMATOR
RONCHI RULING
L1
SPATIAL FILTER
L2
L3
L4
MIRROR
TRANSDUCER
WATER TANK
MIRROR
L5
MICROSCOPE OBJECTIVE
RONCHI RULING
L6
OPTICAL DETECTOR

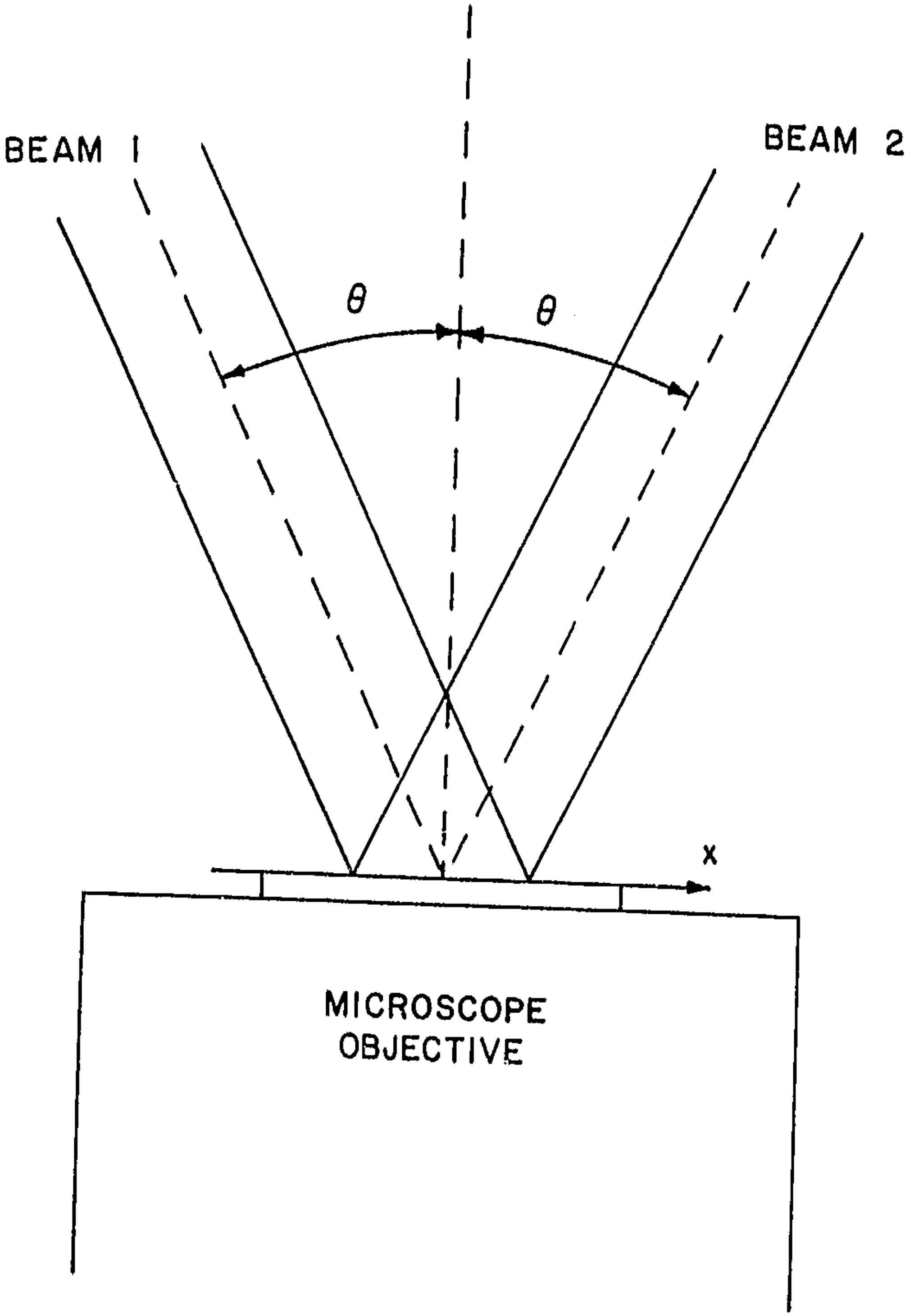
BEAM 1
BEAM 2
θ
θ
X
MICROSCOPE
OBJECTIVE

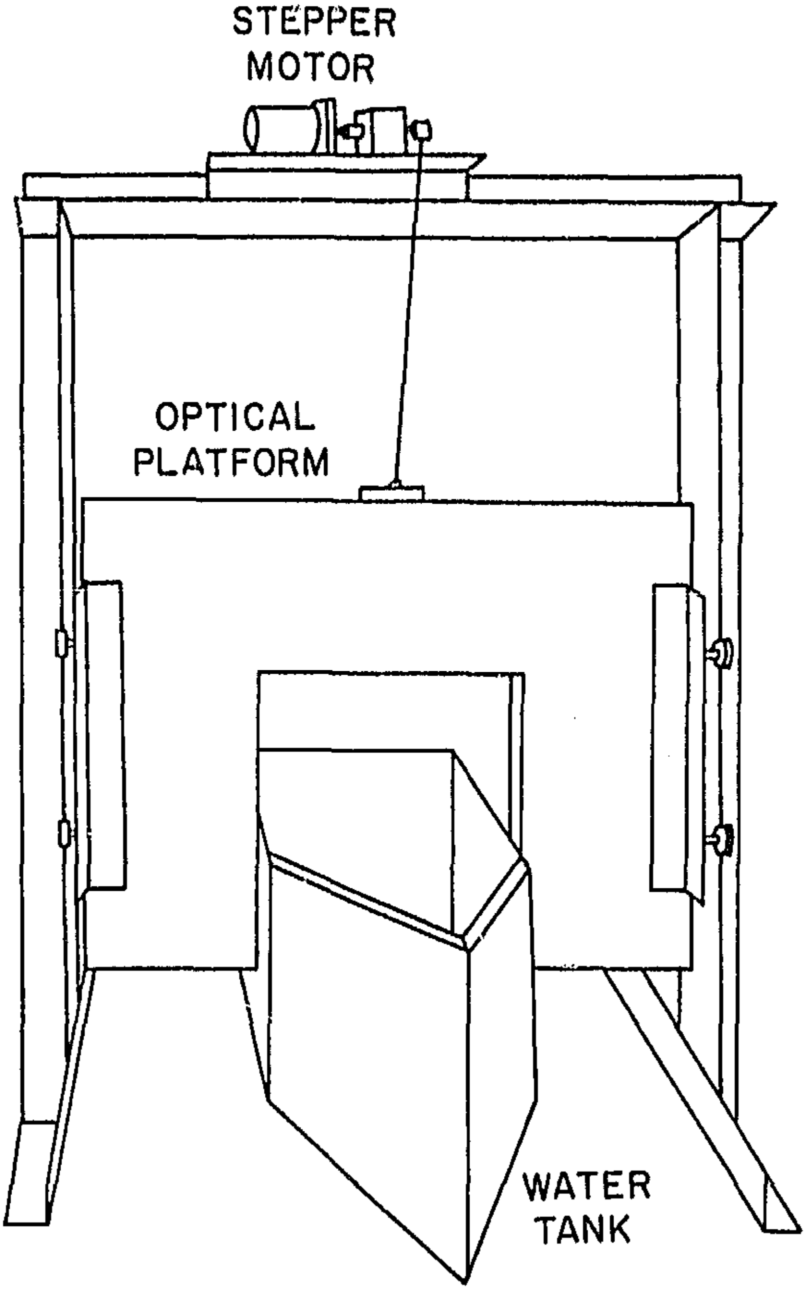
STEPPER
MOTOR
OPTICAL
PLATFORM
WATER
TANK

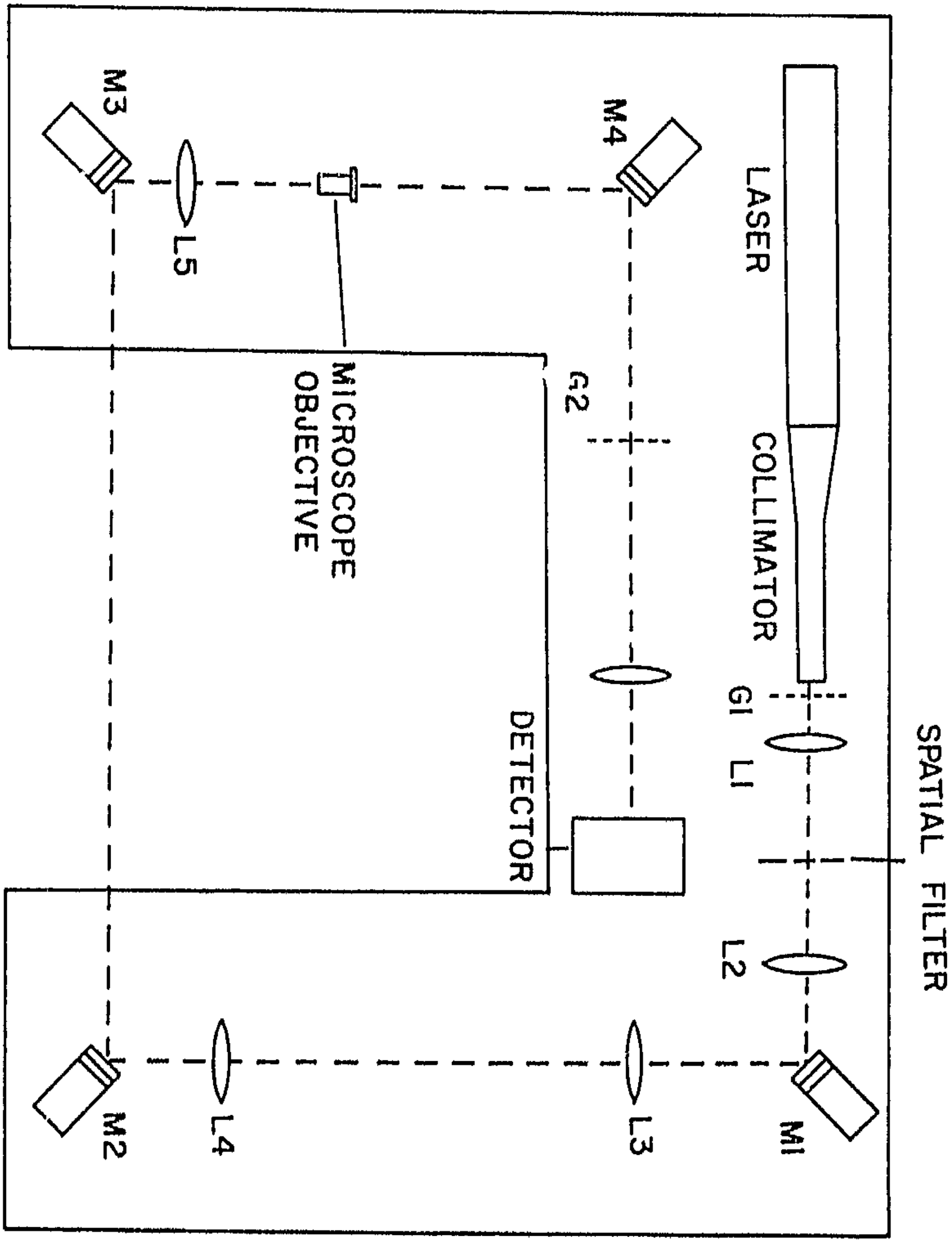
LASER
COLLIMATOR
SPATIAL FILTER
GI
LI
L2
MI
L3
L4
M2
M3
L5
M4
G2
MICROSCOPE OBJECTIVE
DETECTOR

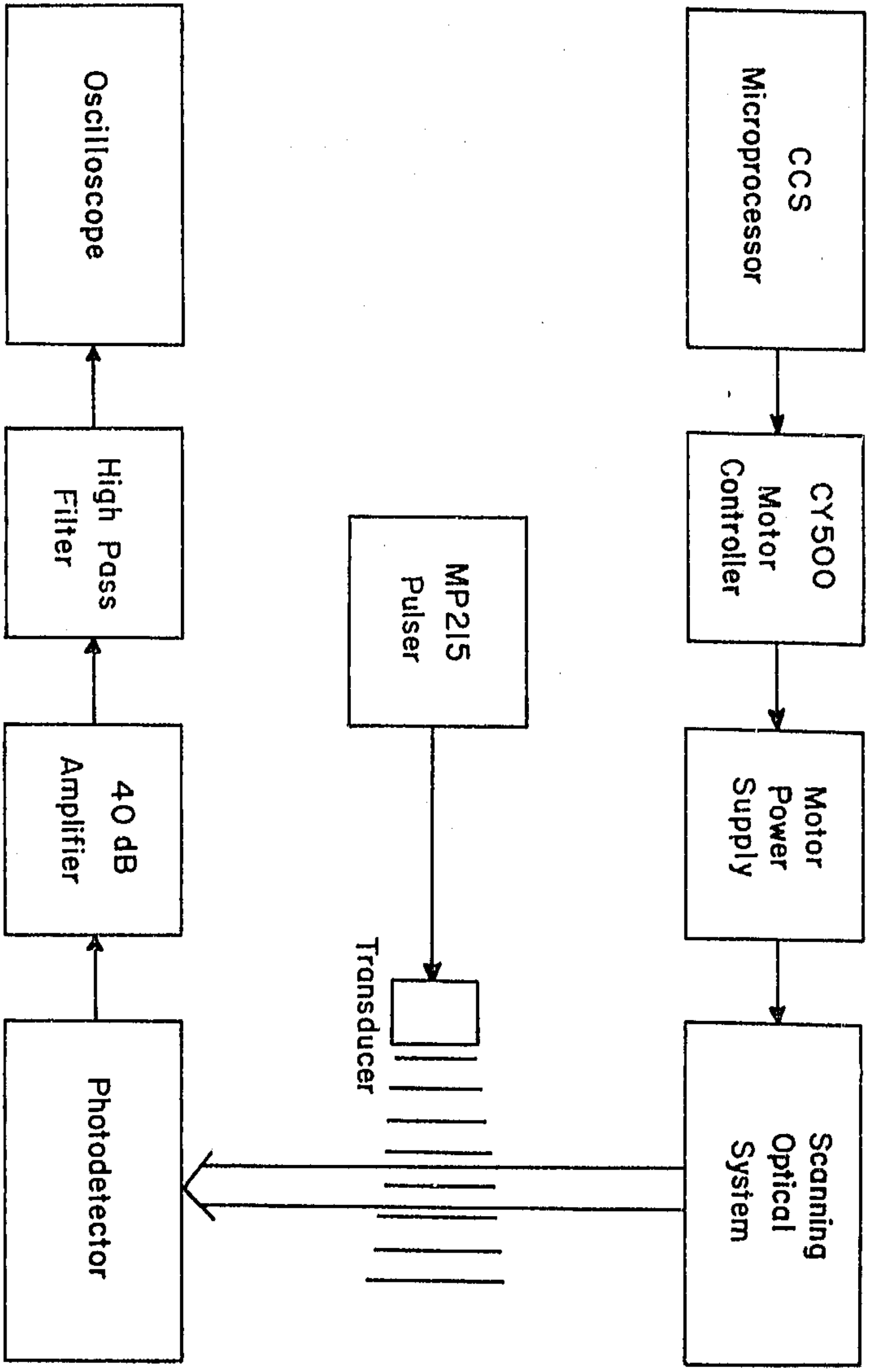
CCS Microprocessor
CY500 Motor Controller
Motor Power Supply
Scanning Optical System
MP215 Pulser
Transducer
Oscilloscope
High Pass Filter
40 dB Amplifier
Photodetector

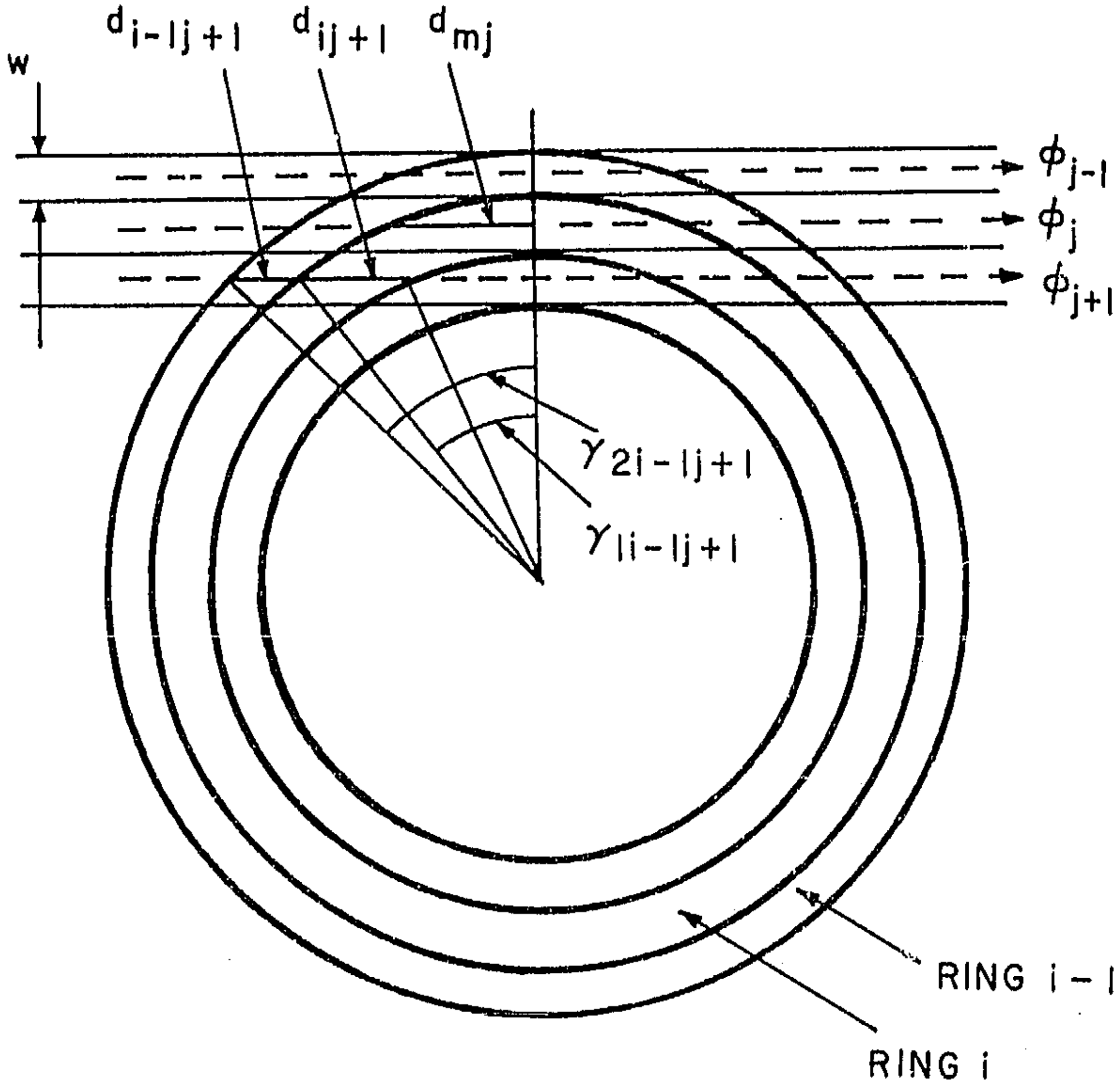
d_{i-1j+1}
d_{ij+1}
d_{mj}
w
ϕ_{j-1}
ϕ_j
ϕ_{j+1}
$\gamma_{2i-1j+1}$
$\gamma_{1i-1j+1}$
RING i − 1
RING i

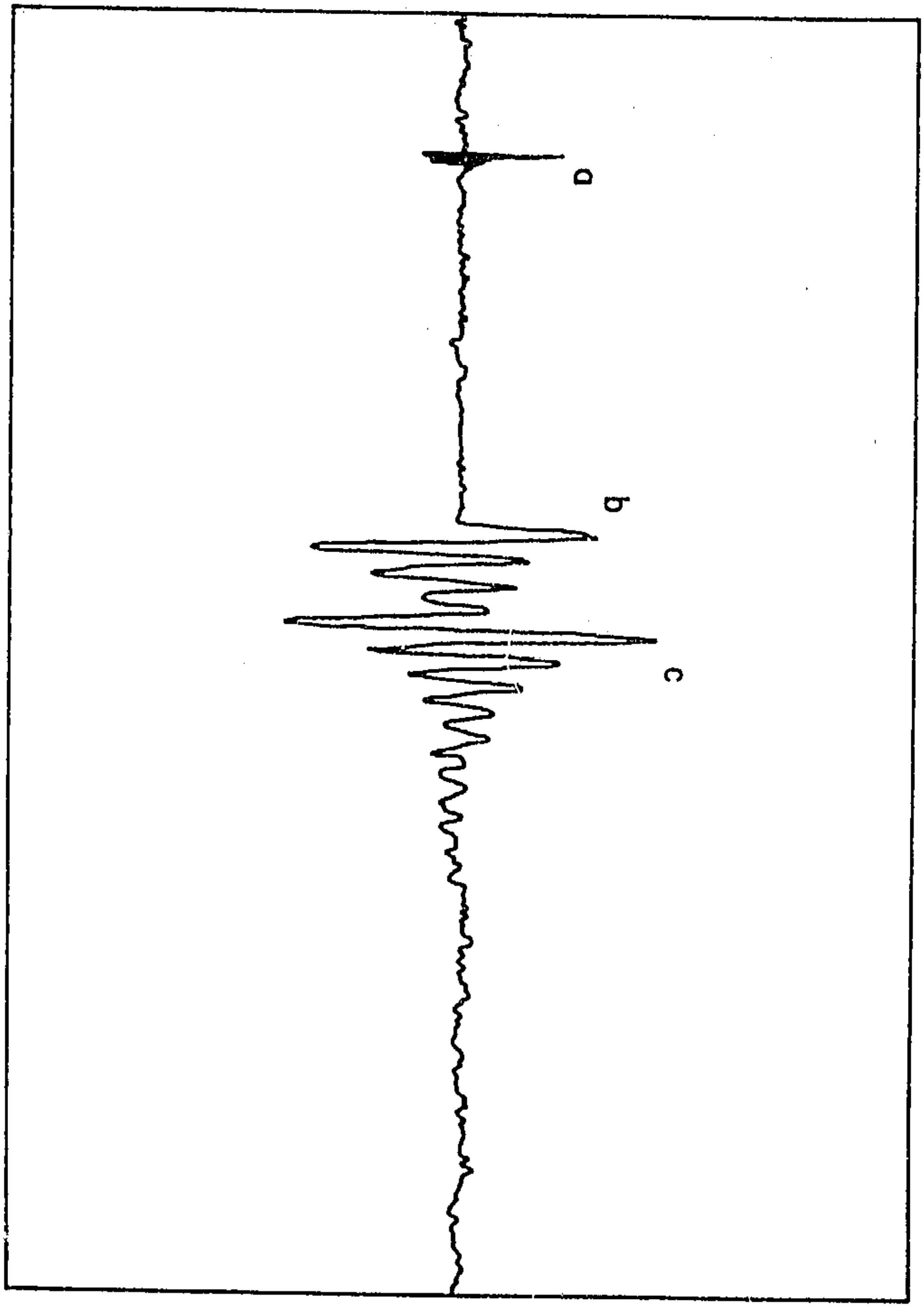
a
b
c

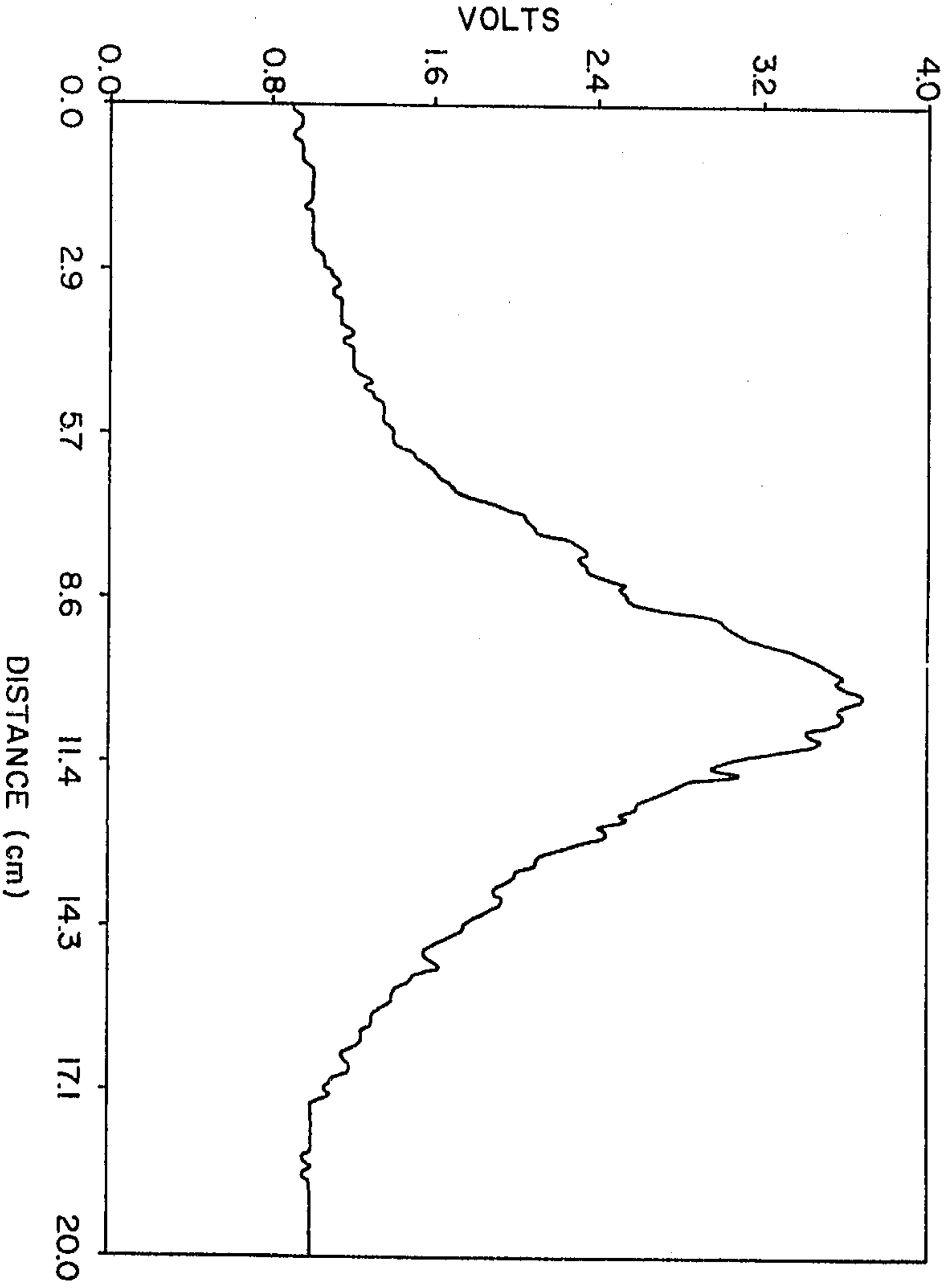
VOLTS
0.0
0.8
1.6
2.4
3.2
4.0
0.0
2.9
5.7
8.6
11.4
14.3
17.1
20.0
DISTANCE (cm)

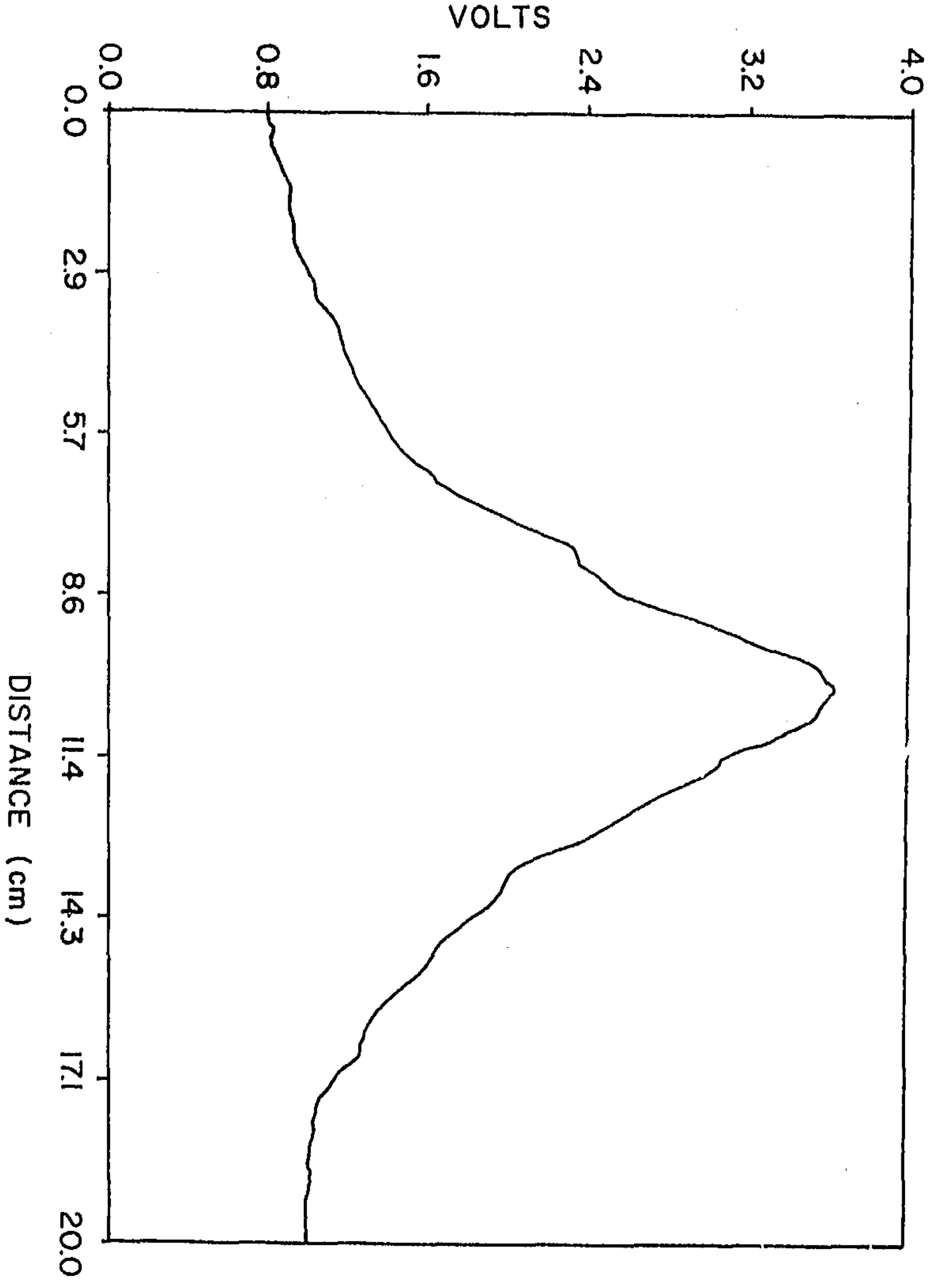
VOLTS
0.0
0.8
1.6
2.4
3.2
4.0
DISTANCE (cm)
0.0
2.9
5.7
8.6
11.4
14.3
17.1
20.0

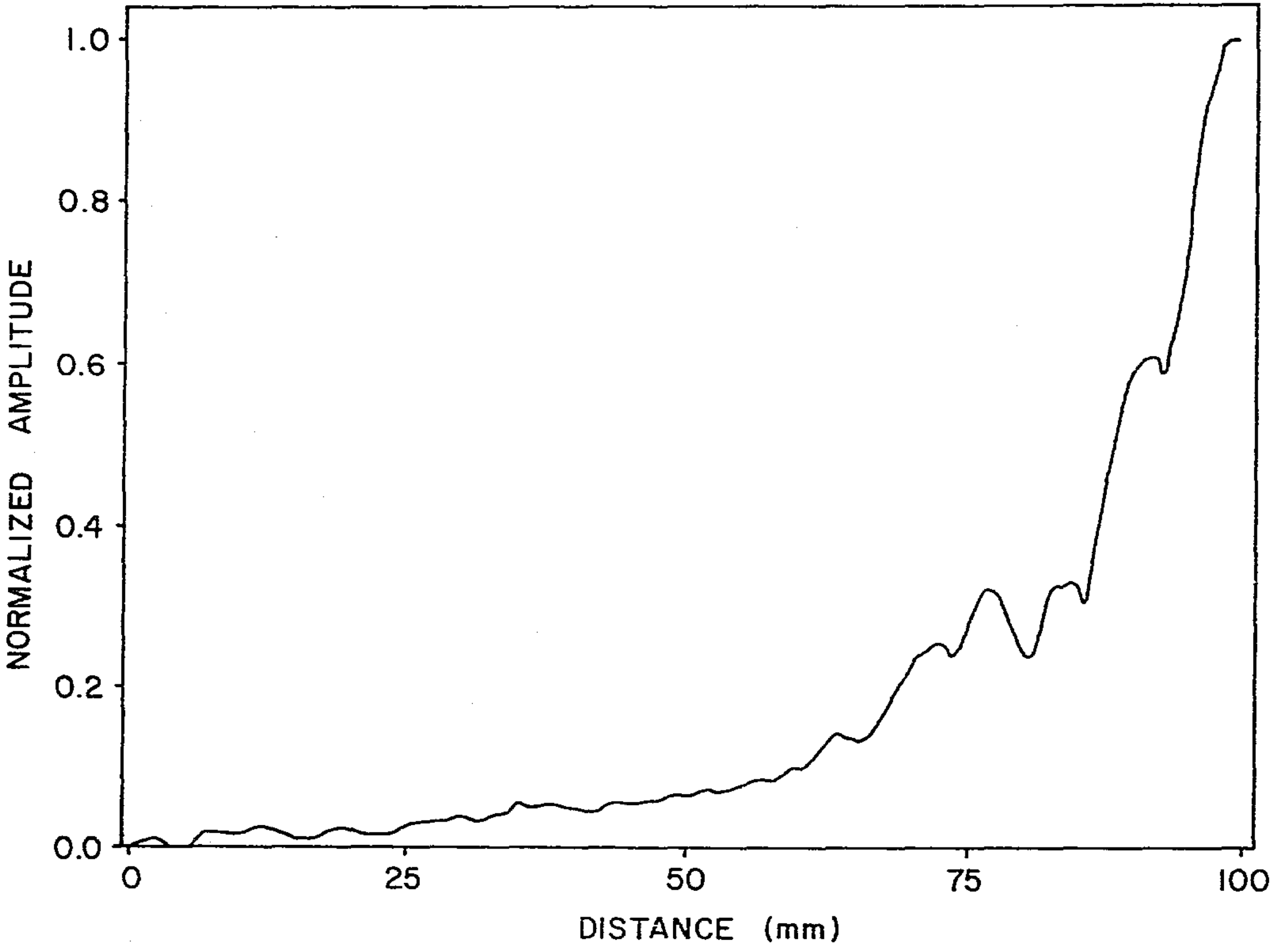
NORMALIZED AMPLITUDE
1.0
0.8
0.6
0.4
0.2
0.0
0
25
50
75
100
DISTANCE (mm)

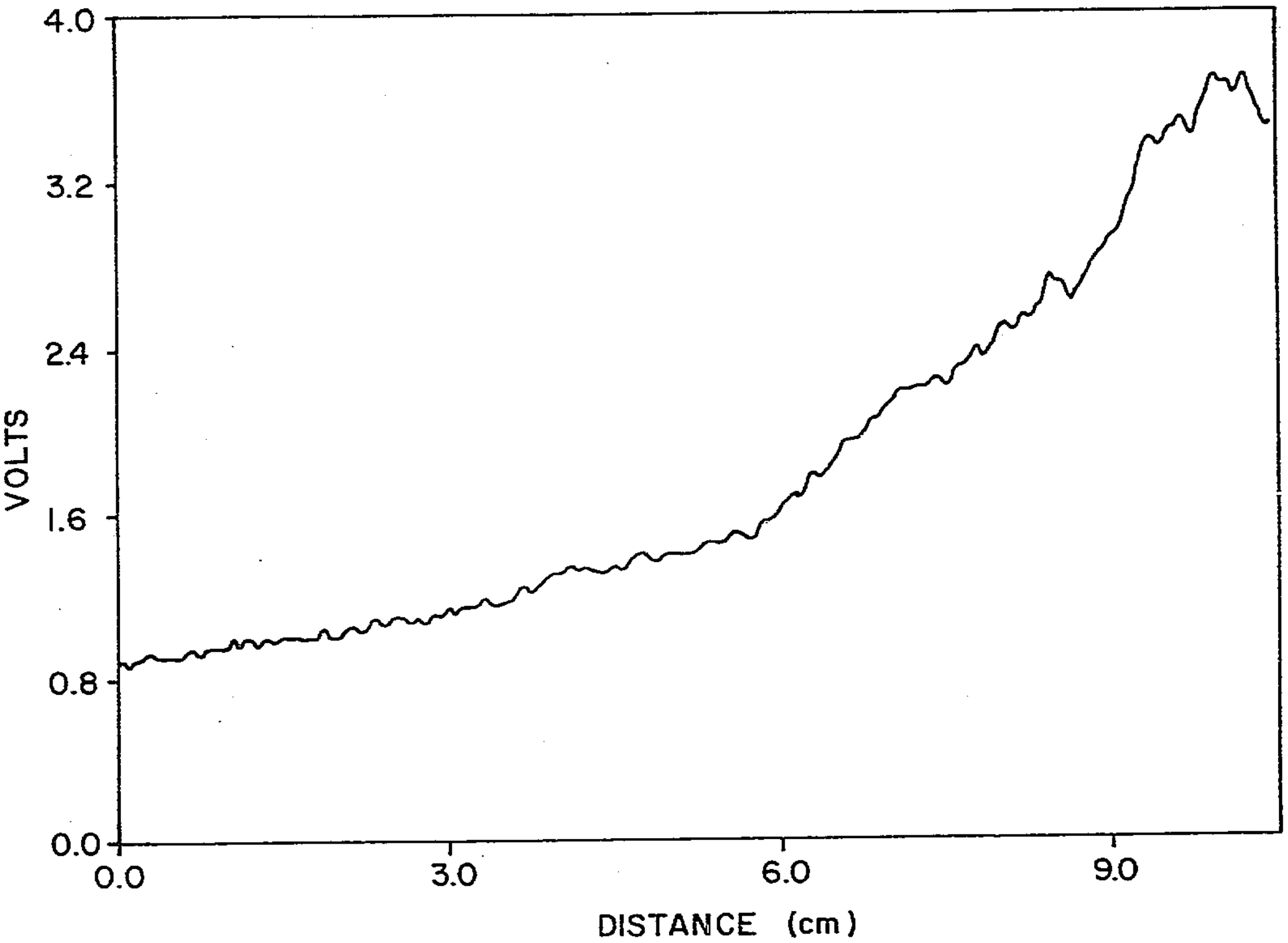
4.0
3.2
2.4
1.6
0.8
0.0
VOLTS
0.0
3.0
6.0
9.0
DISTANCE (cm)

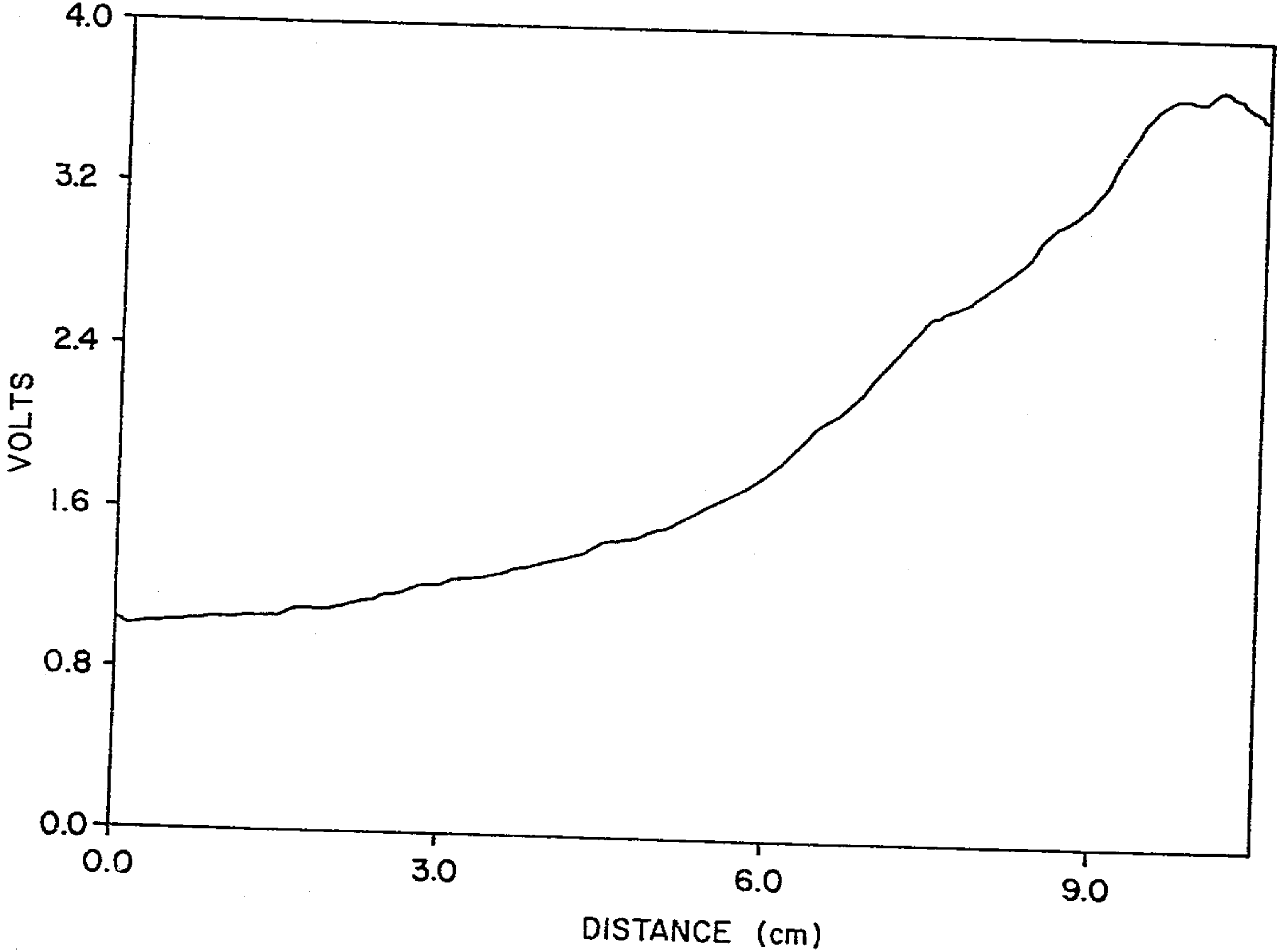
4.0
3.2
2.4
1.6
0.8
0.0
VOLTS
0.0
3.0
6.0
9.0
DISTANCE (cm)

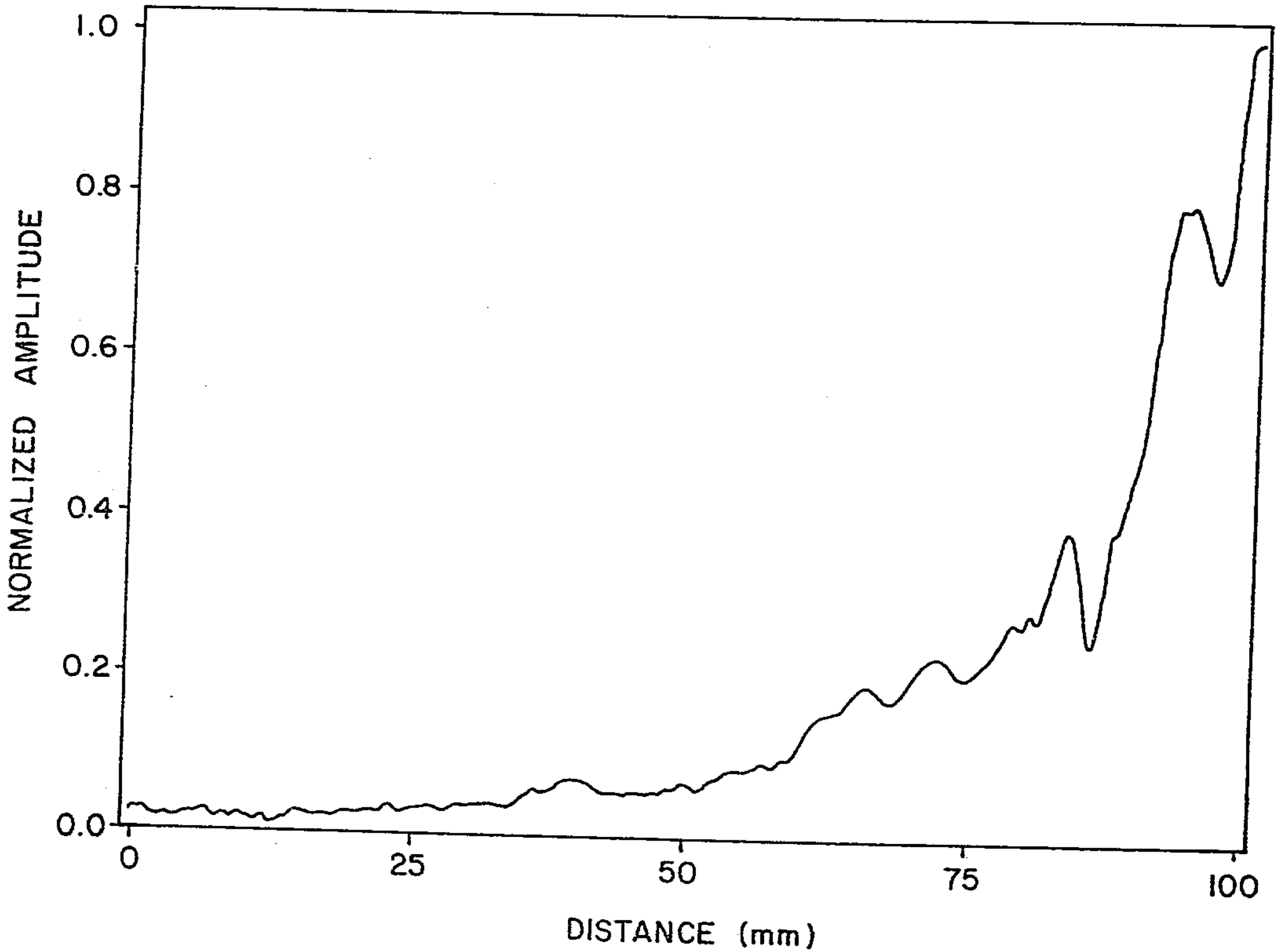
NORMALIZED AMPLITUDE
1.0
0.8
0.6
0.4
0.2
0.0
0
25
50
75
100
DISTANCE (mm)